2009 Ninth International Conference on Intelligent Systems Design and Applications

Intracellular Volume Registration

Shin Yoshizawa [1] Satoko Takemoto [1] Miwa Takahashi [2] Makoto Muroi [1]
Sayaka Kazami [1] Hiromi Miyoshi [1] Hideo Yokota [1]

[1] RIKEN, 2-1, Hirosawa, Wako, Saitama, 351-0198, Japan
[2] University of Geneva, 30 quai Ernest-Ansermet, 1211, Geneva, Switzerland
{shin, satoko-t, mmuroi, sayaka, hiromi-miyoshi, hyokota}@riken.jp Miwa.Umebayashi@unige.ch

***Abstract*—The paper proposes a novel 3D image registration approach to calculating intracellular volumes. The approach extends a standard image registration framework to the curved cell geometry. An intracellular volume is mapped onto another intracellular domain by using two pairs of point set surfaces approximating their nuclear and plasma membranes. The approach is implemented to an interactive volume registration system. We demonstrate that our approach can create models of cells with multiple organelles from data collected from living cells.**

Keywords-intracellular volume; live cell imaging; non-rigid registration; least-squares RBF

I. Introduction

Recent advances in live cell imaging make it possible to observe the organelles[1] in living cells as 3D images. Quantitative analysis of such *intracellular volumes* has thus become important in cell biology [1]. Also numerical simulations based on the intracellular volumes are becoming popular in recent biophysics and systems biology. Therefore, to construct the integrated multiple organellar models has considerable attentions to interconnecting the models and traditional biology experiments [2]. Intracellular volumes are usually determined under a confocal laser microscope with fluorescent organellar markers. Unfortunately, simultaneous observation of many different fluorescent markers[2] is not possible because of technical difficulties with microscopes, fluorescent markers, and cell conditions ([3], [4], and references therein).

In this paper, we propose a novel approach to *intracellular volume registration* (the non-rigid alignment of separately observed 3D images of the different intracellular objects) as an alternative solution to overcoming the difficulties of simultaneous observation. The main idea behind the approach is to construct a function that maps one intracellular domain to another by using the geometric feature points extracted from the cell's nuclear and plasma membranes. First, we observe the cytosol together with its nucleus as a reference volume, and simultaneously the objective organelle as its corresponding target volume. The cytosol and nucleus are chosen because their topological configuration during interphase, that of a sphere enveloping another sphere, is simple. Then these regions are isolated from their backgrounds to produce segmented reference volumes. Next, the nuclear and plasma membranes are approximated by a pair of point set surfaces sampled on the boundaries of the isolated regions, and their geometric features are extracted. Finally, a mapping function between a pair of reference volumes is constructed by applying affine transformation, least-squares radial basis function (RBF) fitting, and tetrahedral barycentric interpolation methods to the extracted features. Figure 1 illustrates our approach.

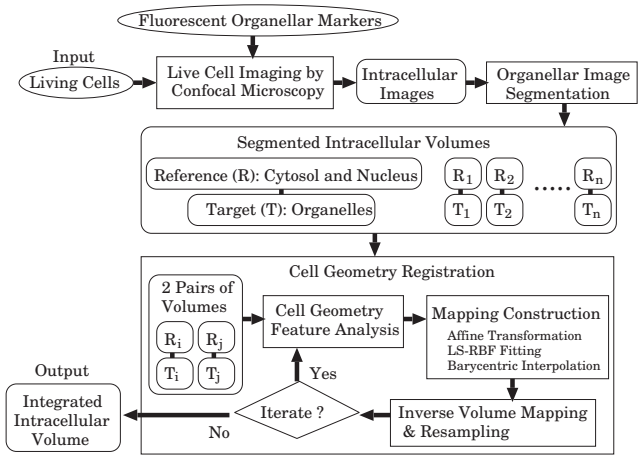

Figure 1. Intracellular volume registration flowchart.

The goal of this study was to generate a numerical cell model consisting of multiple organelles that represents living cell as close as possible. Such a model is useful for presenting combined organellar information to biologists and for running numerical cell simulations. Our approach is capable of integrating individually observed intracellular

[1]For simplicity, we use a word of *organelle* for objects in living cells such as organelles, cytoskeletons, vesicles, etc.

[2]Only one or two fluorescent markers are usually employed in cell biology experiments to avoid the problems caused by increasing markers.

978-0-7695-3872-3/09 $26.00 © 2009 IEEE
DOI 10.1109/ISDA.2009.42

objects, as demonstrated in Section V. The study presents a new approach to overcoming the difficulties of simultaneous observation of many different fluorescent markers. Its technical contribution includes a novel method for extracting cell geometry features; this method semi-automatically provides feature point correspondences.

S.Y. and H.Y. developed the registration technique and S.T. and H.Y. developed the segmentation technique. The other authors were devoted to obtain the input intracellular volumes.

The rest of paper is organized as follows. Section II briefly describes previous work on image registration. We present how to segment reference and target volumes in Section III. Section IV describes the cell geometry registration technique. Our numerical experiments are explained in Section V. We conclude the paper in Section VI.

II. Previous Work on Image Registration

Image registration is popular and well-studied in computer vision and image processing communities; see [5], [6], and references therein for general image registration techniques. The high-dimensional extensions of such techniques are often used in bio-medical image processing [7]–[9] to merge CT, MRI, and microscopic images. Non-rigid transformations are necessary for such bio-medical data because of the complex curved geometry of the objects of study. In particular, traditional RBF fitting methods have been used for non-rigid registration [10]–[12] and many other tasks. On the other hand, non-rigid transformations for intracellular volumes had not been studied until very recently [13]–[15] because the objects in living cells are usually not solid; they are also both topologically and geometrically complex and vary with time. Therefore, intracellular volume registration is a difficult problem, but it is a promising research subject because of rapid advances in live-cell-imaging technology.

Mattes et al. employed a thin-plate spline transformation model with landmarks for their 2D intracellular image registration [13]. Kim et al. proposed a non-rigid registration approach to intracellular volumes of different cell nuclei [14]; the approach was based on the so-called demons algorithm [16]. Yang et al. extended this approach to segmented volumes [15]. However they considered only cell nuclei, which, unlike nuclear and plasma membranes, have a simple topological and geometrical configuration. Our approach is capable of transforming a volume domain (including organelles) between the nuclear and plasma membranes, whereas the previous approaches [13]–[15] consider only the volume domain inside the nucleus (with no organelles).

In contrast with the previous RBF techniques [10]–[12] used in CT and MRI image registration, our approach employes a least-squares RBF fitting method that is popular in surface reconstruction [17].

III. Intracellular Image Segmentation

To construct a function mapping one volume onto another, we first isolate the nuclear and cytosolic regions from their backgrounds. The target organellar region within the cytosol is segmented for further quantitative analysis, although the segmented target volume is not necessary to construct the mapping function.

The intracellular volumes generated from observations of living cells contain noise. Their low signal-to-noise ratio has causes, including poor microscope resolution, Brownian motion, blurring, movement of organelles, and bleaching of fluorescent markers [4]. Moreover, small variations made to the observation settings for different organelles introduce inconsistencies in the same feature among images. Such noise and inconsistency make it difficult to achieve high-quality segmentation of intracellular volumes. Our segmentation technique incorporates noise reduction methods and clusters the filtered image.

Image details are important in isolating organelles for quantitative analysis. On the other hand, image smoothness and robustness to small perturbations are required for segmenting the nucleus and cytosol in order to construct a good mapping function. Therefore, we use two image denoising filters for the targets (organelles) and their corresponding references (cytosol and nucleus): Non-Local Means (NL-Means) [18] for targets and the Block-Median Pyramidal Transform (BMPT) [19] for the references. BMPT filter produces nicely smoothed volumes, and its multiresolution strategy provides robustness. NL-Means filter preserves detail while reducing noise.

After the filters are applied, the cytosolic, nuclear, and background regions are segmented by unsupervised K-mean clustering [20] for the filtered image intensities. Finally, the unwanted isolated regions are labeled and merged to reproduce the topological configuration of cytosol and nucleus. Figure 2 shows the isolation of the nucleus and cytosol from their backgrounds.

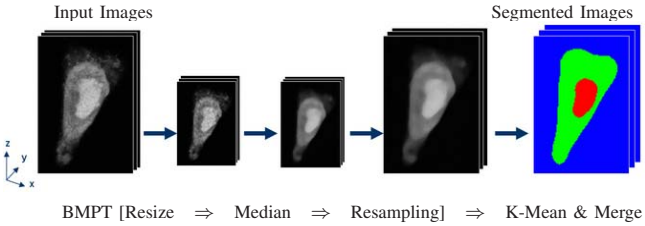

Figure 2. Segmentation of cytosol and nucleus.

IV. Cell Geometry Registration

Our registration technique is based on extending a standard image registration framework [6] to the curved cell geometry. First, the geometric features of each reference volume are extracted. Next, a mapping function f :

$(u,v,w) \rightarrow (x,y,z)$ between two different intracellular domains $(u,v,w) \in \Omega_1$ and $(x,y,z) \in \Omega_2$ is constructed by using a pair of reference volumes. Next, one of the target organellar volumes is mapped onto another target domain via the constructed mapping function, and then the mapped organellar volume is resampled. Finally, the resampled volume is integrated to another volume (Fig. 3). The following mapping methods are implemented in our interactive intracellular volume registration system (Fig. 9).

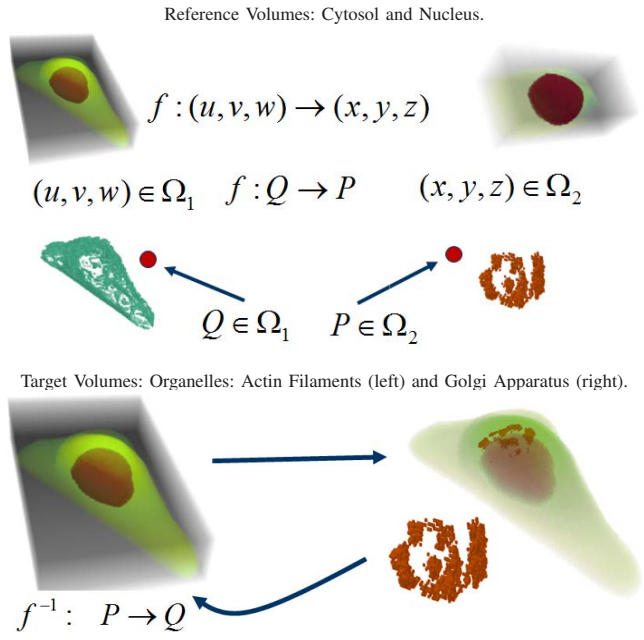

Figure 3. Intracellular mapping. Here a mapping function f, which transforms a point $Q \in \Omega_1$ to a corresponding point $P \in \Omega_2$, is constructed from two reference volumes. The inverse mapping f^{-1} maps the target organelle (Golgi apparatus) to the domain of another cytoskeleton (Actin filaments).

A. Cell Geometry Feature Analysis

Consider a given pair of plasma membranes represented by the point set surfaces ∂_1 and ∂_2, which live in domains Ω_1 and Ω_2, respectively. Let $\mathbf{c}_1$ and $\mathbf{c}_2$ be the centers of gravity of ∂_1 and ∂_2, respectively. Principal Component Analysis (PCA) of ∂_1 and ∂_2 gives us the pair of corresponding principal axes $\{\mathbf{t}_1^1, \mathbf{t}_2^1, \mathbf{t}_3^1\}$ and $\{\mathbf{t}_1^2, \mathbf{t}_2^2, \mathbf{t}_3^2\}$, respectively. The same computations are applied to the corresponding nuclear membranes. Then the following feature and sub-feature points are extracted for the two pairs of nuclear and plasma membranes (four point set surfaces).

Let ∂, $\mathbf{c}$, and $\{\mathbf{t}_1, \mathbf{t}_2, \mathbf{t}_3\}$ be one of the point set surfaces, its center of gravity, and its principal axes, respectively. Assume that $\mathbf{t}_1$ is the longest PCA direction of ∂, and $\mathbf{t}_3$ is perpendicular to the cell face on the cover-glass. We consider three feature point sets sampled on ∂: the intersection points between ∂ and the 6, 26, and 11 rays from $\mathbf{c}$, respectively shown in the left, center, and right images of Figure 4. The first two sets are easily calculated from the PCA directions. The last set is specialized to a triangle-patterned[3] cell shape, where the corresponding 11 rays are parallel to $\pm\mathbf{t}_{2,3}$, $\chi(\mathbf{t}_1)$, $\pm\mathbf{t}_{2,3} + \chi(\mathbf{t}_1)$, and $\chi(\pm\mathbf{t}_2 - \mathbf{t}_1)$, where $\chi(\mathbf{t}) = (\text{argmax}_{\mathbf{x}\in\partial} < \mathbf{x}-\mathbf{c}, \mathbf{t} >)-\mathbf{c}$. Here the vector function $\chi(\mathbf{t})$ gives us the farthest direction with respect to a given vector $\mathbf{t}$, and the multiple sub-index $\mathbf{t}_{i,j}$ corresponds to $\mathbf{t}_i$ and $\mathbf{t}_j$. The sub-feature points are sampled on the geodesics between the feature points on ∂.

Note that the correspondences between two sets of feature points on ∂_1 and ∂_2 are automatically obtained by specifying the correspondence of the PCA directions $\{\mathbf{t}_1^1, \mathbf{t}_2^1, \mathbf{t}_3^1\}$ and $\{\mathbf{t}_1^2, \mathbf{t}_2^2, \mathbf{t}_3^2\}$, because the feature points (also sub-feature points) are automatically generated after the PCA directions are obtained. This semi-automatic correspondence generation reduces a lot of manual registration, and it gives us an intuitive and interactive user interface, as shown in Figures 4, 7, and 8.

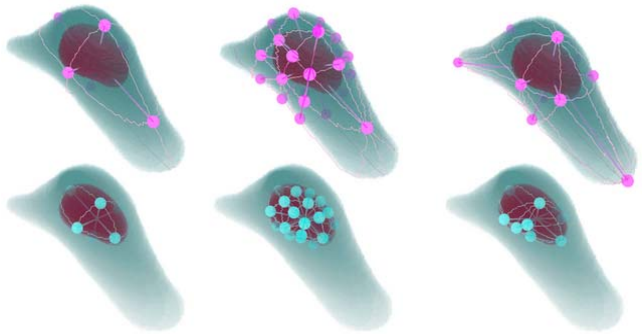

Figure 4. Extracted feature and sub-feature points based on PCA of nuclear (bottom) and plasma (top) membranes.

B. Affine Transformation with PCA

Besides the affine transformation via a corresponding pair of four points manually specified on the plasma membrane surfaces, the affine transformation $f(\mathbf{x})$, which transforms a point $\mathbf{x} \in \Omega_1$ to the domain Ω_2, is automatically constructed via PCAs of ∂_1 and ∂_2:

$$f(\mathbf{x}) = \mathbf{A}(\mathbf{x} - \mathbf{c}_1) + \mathbf{c}_2, \quad \mathbf{A} = (\mathbf{t}_1^2, \mathbf{t}_2^2, \mathbf{t}_3^2)(\mathbf{t}_1^1, \mathbf{t}_2^1, \mathbf{t}_3^1)^{-1}.$$

C. Least-Squares RBF Fitting

To fit the RBF robustly, we use the least-squares RBF formulation. Consider the so-called RBF centers $\{\mathbf{c}_j\}$, which consist of one of the feature point sets in Ω_1 and the bounding box vertices of the cytosol and nucleus (Fig. 8, right). Let $\mathbf{p}$ be a set of feature and sub-feature points of

[3]We employed a triangle micro-patterned substrate in experiments because it reduces complexity of plasma membrane shape, besides two triangles, whose vertices are corresponded each other, determine a unique affine transformation matrix.

the cytosol and nucleus in Ω_1 (two point set surfaces) and let $\mathbf{q}$ be the corresponding set of feature and sub-feature points in Ω_2. Then, the LS-RBF is given by

$$f(\mathbf{x}) = \sum_j \lambda_j \Phi(|\mathbf{x} - \mathbf{c}_j|) + g(\mathbf{x}),$$

where $\Phi(u) = u^3$, $g(\mathbf{x})$ is a linear polynomial, and the RBF coefficients $\lambda = \{\lambda_j\}$ are obtained by solving a least-squares system of linear equations $\lambda = (\mathbf{A}^T\mathbf{A})^{-1}\mathbf{A}^T\mathbf{q}$. Here the rectangular matrix $\mathbf{A}$ is composed by satisfying

$$f(\mathbf{p}) = \mathbf{q}, \qquad \sum_j \lambda_j g(\mathbf{p}) = 0.$$

The resulting RBF is the so-called pseudo-cubic function [21]. The linear regression RBF scheme [22] is used as $\mathbf{A} \Rightarrow (\alpha\mathbf{I} + \mathbf{A})$ to reduce self-intersections, where $\mathbf{I}$ is an identity matrix and α is a user-specified smoothness parameter. Figure 5 shows the volumes and boundary sets mapped via LS-RBF.

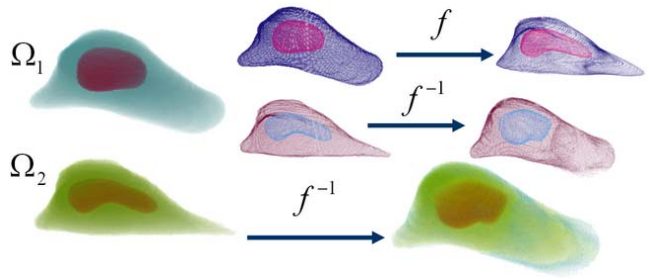

Figure 5. LS-RBF fitting with inverse mapping. Left: two pairs of cytosol with nucleus. Center: boundary point sets approximating the plasma and nuclear membranes. Right: point sets and volume transformed via the LS-RBF f and its inverse mapping f^{-1}.

D. Tetrahedral Barycentric Interpolation

Valid tetrahedrization can be applied to the bounding boxes of the cytosol and nucleus without any degeneration of a tetrahedron because of its topological configuration such as a sphere enveloping another sphere (Fig. 6).

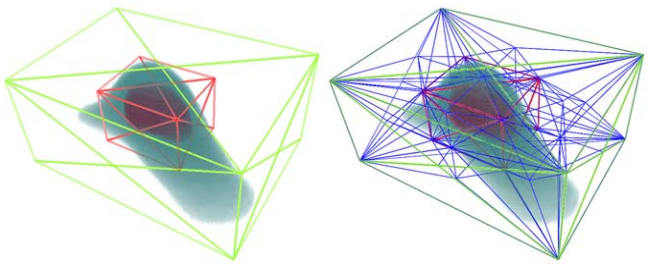

Figure 6. Tetrahedrization example: the cytosolic and nuclear bounding boxes (left) and the tetrahedrization (right).

Six hexahedra are generated by connecting the corresponding corners of the nuclear and cytosolic bounding boxes (Fig. 6, left). The tetrahedrization consists of seven hexahedra (the generated six plus the nucleus bounding box), each of which consists of 24 tetrahedra. The tetrahedra in each hexahedron are generated by adding a point to the hexahedron center and six points to its face centers, and then connecting these points with the hexahedron vertices.

The mapping function between a pair of tetrahedrizations in Ω_1 and Ω_2 is constructed by a set of tetrahedral barycentric interpolations. The location of a point inside of the tetrahedron is given by the volume ratio of four tetrahedra as a generalization of 2D triangle barycentric coordinates.

E. Interactive Registration System

We have developed a computer-aided registration system based on our registration technique. The system is implemented by using Java Development Kit with Java3D. Figure 7 illustrates a graphical user interface (GUI) of the system.

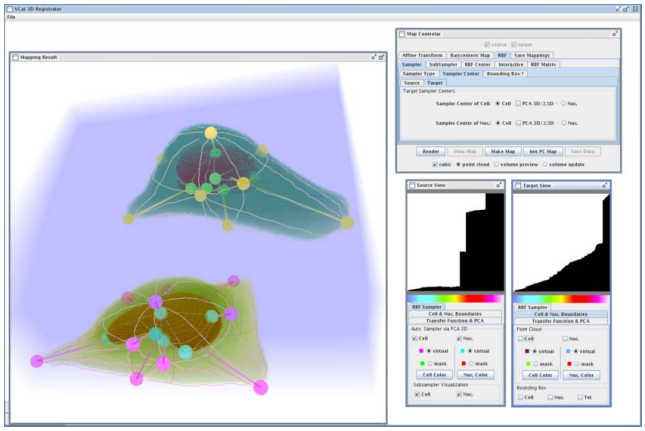

Figure 7. Interactive registration system GUI.

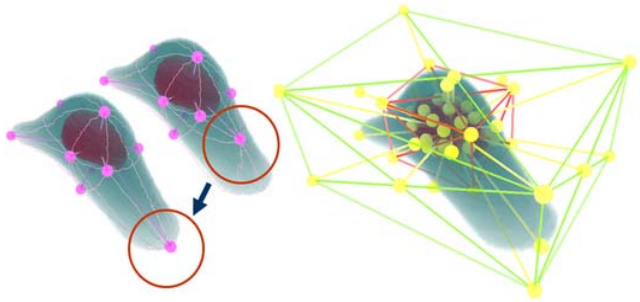

Figure 8. Our system includes an interactive GUI (left) and automatic RBF center generation (right).

The system includes a 3D volume rendering window in order to visualize input reference volumes. This 3D rendering window provides the interactive GUI to repositioning the feature points restricted on the nuclear and plasma membrane surfaces of the cell (Fig. 8, left). Changes of visualization and registration settings by a user are immediately

reflected on the 3D rendering window. Then, the system performs the cell geometry feature extraction method and the mapping methods described above. Finally, the system updates the 3D rendering window according to the results of the methods. Figure 9 illustrates an abstracted architecture of the system. This interactive system provides intuitive registration of intracellular volumes.

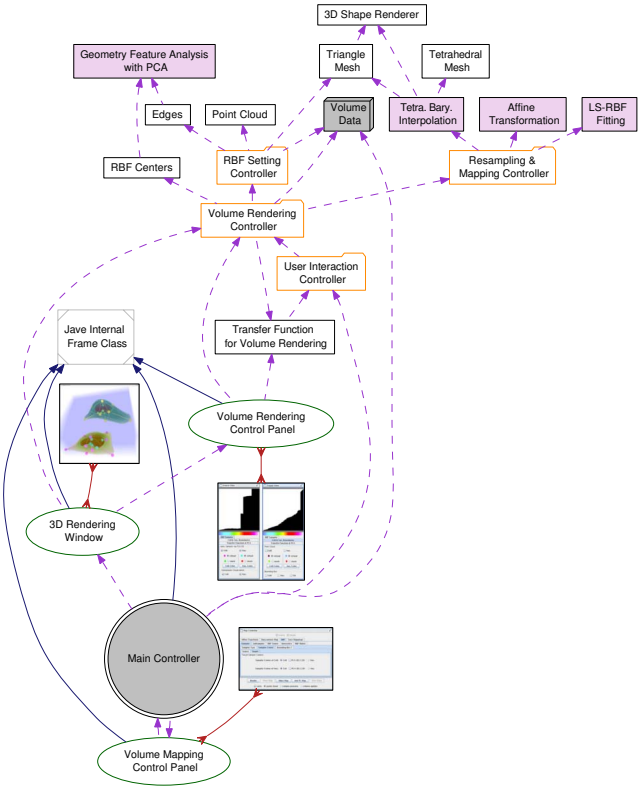

Figure 9. System architecture consists of controllers (orange box), classes (black box), GUI panels (green ellipse), and the methods described above (pink box). The blue and purple arrows represent inheritance and collaboration relations, respectively.

V. Results

In experiments, we used HeLa cells cultured on a triangular micro-patterned substrate produced by the photochemical method [23] to regularize the observed living HeLa cell shapes. A fluorescent-protein-tagged nuclear localization signal (NLS) plasmid was employed to characterize the cytosol and nucleus. The parameters of the BMPT and NL-Means for different organelles were decided on by cell biologists, who selected the result that they considered to be the best approximation of the organelles by using varying parameters to filter the results. All numerical experiments were performed on a Core2Duo PC (2.4 GHz, no parallelization is used) with 8 GB RAM.

Figures 3, 10, and 11 show our registration results, in which the resulting volumes consist of 304x508x116 voxels.

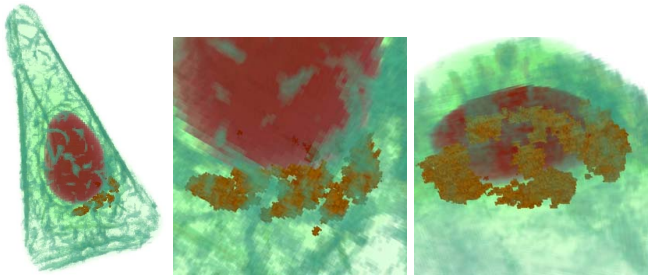

Figure 10. Two organellar volumes (Actin filaments and Golgi apparatus) are combined where the corresponding reference volumes are shown in Figure 3.

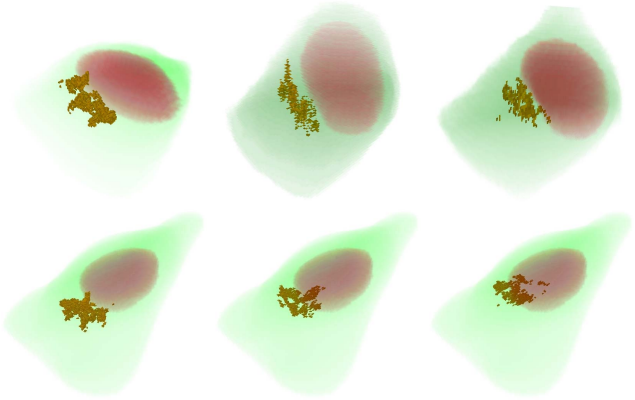

Figure 11. Examples of registration by our approach. Three different Golgi apparatus volumes (top) are successfully mapped onto another reference volume (bottom). The top three volume data were collected from one living cell with varying time.

The shapes and positions of the mapped organellar volumes are reasonable, even though the geometric configurations of the cytosol and nucleus are complex. The resulting volumes provide us the combined geometry and positions of organelles among the individually observed cells. For example, we can easily see the relative positions of cytosol, nucleus, and Golgi apparatus among varying time in the bottom images of Figure 11, whereas these relationships are not clear in the top images because of different nuclear and plasma membrane shapes. This is an advantage over raw image data and the previous intracellular image registration approaches [8], [13]–[15] for analyzing organellar dynamics and functions. Unlike the landmarks used in [13] and the image intensity of cell nuclei employed in [14], [15], our approach does not depend on the target organellar volumes explicitly. Therefore, our registration results are much robust with respect to topology changes of observation targets which biologist would like to analyze. Note that the techniques of [14], [15] are not able to merge the organelles. Compared with recent image registration techniques [9], [11], [12], our approach is preferable for mapping intracellular volumes because of our method for extracting cell geometry features.

Our use of the point set surfaces gives us the interactive registration rate (about 1-10 microseconds) for the computations that require user manipulation, such as adjustments to the corresponding points in the LS-RBF fitting. The inverse volume resampling requires a few minutes. One intracellular volume registration task can be completed within 5-20 minutes by an experienced user with our system.

VI. Conclusion

In this paper, we proposed a novel approach to intracellular volume registration based on constructing a function mapping one intracellular volume onto another by analyzing the geometry of the plasma and nuclear membranes. This approach allows us to integrate the volumes of individually observed organelles, which is difficult in conventional live cell imaging. We presented three mapping methods (affine transformation, least-squares radial basis function fitting, and tetrahedral barycentric interpolation) specialized to intracellular volumes. The interactive intracellular volume registration system was also developed. Besides its benefits to quantitative analysis in cell biology, our approach is useful for cell simulations based on real-world data.

Future work includes registration during cell division and incorporating physically based transformations.

Acknowledgements

This work was supported in part by Strategic Programs for R&D (President's Discretionary Fund) of RIKEN and Grants-in-Aid for Scientific Research of Japan (19800062, 20700175, and 20113007).

References

[1] R. Eils and C. Athale, "Computational imaging in cell biology," *J. Cell Biol.*, vol. 161, pp. 477–481, 2003.

[2] C. Priami, "Algorithmic systems biology," *Communications of the ACM*, vol. 52, no. 5, pp. 80–88, 2009.

[3] R. D. Goldman and D. L. Spector, *Live Cell Imaging: A Laboratory Manual*. Cold Spring Harbor Laboratory Press, 2004.

[4] H. Bhaskar and S. Singh, "Live cell imaging: a computational perspective," *J. of Real-Time Image Processing*, vol. 1, pp. 195–212, 2007.

[5] B. Zitová and J. Flusser, "Image registration methods: A survey," *Image and Vision Computing*, vol. 21, no. 11, pp. 977–1000, 2003.

[6] B. Zitová, J. Flusser, and F. Šroubek, "Image registration: A survey and recent advances," in *Tutorial of IEEE International Conference on Image Processing*. IEEE, 2005, pp. 1–2.

[7] J. B. A. Maintz and M. A. Viergever, "A survey of medical image registration," *Medical Image Analysis*, vol. 2, no. 1, pp. 1–16, 1998.

[8] B. Rieger, C. Molenaar, R. W. Dirks, and L. J. V. Vliet, "Alignment of the cell nucleus from labeled proteins only for 4D in vivo imaging," *Microsc. Res. Tech.*, vol. 64, no. 2, pp. 142–150, 2004.

[9] O. Schmitt, J. Modersitzki, S. Heldmann, S. Wirtz, and B. Fischer, "Image registration of sectioned brains," *International Journal of Computer Vision*, vol. 73, no. 1, pp. 5–39, 2007.

[10] M. Fornefett, K. Rohr, and H. S. Stiehl, "Elastic registration of medical images using radial basis functions with compact support," in *Proc. of IEEE Conference on Computer Vision and Pattern Recognition*, 1999, pp. 402–407.

[11] T. Rhee, J. P. Lewis, K. Nayak, and U. Neumann, "Adaptive non-rigid registration of 3D knee MRI in different pose spaces," in *IEEE International Symposium on Biomedical Imaging*. IEEE, 2008, pp. 1111–1114.

[12] A. M. Siddiqui, A. Masood, and M. Saleem, "A locally constrained radial basis function for registration and warping of images," *Pattern Recognition Letter*, vol. 30, no. 4, pp. 377–390, 2009.

[13] J. Mattes, J. Nawroth, P. Boukamp, R. Eils, and K. M. Greulich-Bode, "Analyzing motion and deformation of the cell nucleus for studying co-localizations of nuclear structures," in *IEEE International Symposium on Biomedical Imaging*. IEEE, 2006, pp. 1044–1047.

[14] I.-H. Kim, S. Yang, P. L. Baccon, E. Heard, Y.-C. Chen, D. Spector, C. Kappel, R. Eils, and K. Rohr, "Non-rigid temporal registration of 2d and 3d multi-channel microscopy image sequences of human cells," in *IEEE International Symposium on Biomedical Imaging*. IEEE, 2007, pp. 1328–1331.

[15] S. Yang, D. Köhler, K. Teller, T. Cremer, P. L. Baccon, E. Heard, R. Eils, and K. Rohr, "Nonrigid registration of 3-D multichannel microscopy images of cell nuclei," *IEEE Trans. on Image Processing*, vol. 17, no. 4, pp. 493–499, 2008.

[16] J. P. Thirion, "Image matching as diffusion process: an analogy with Maxwell's demons," *Medical Image Analysis*, vol. 2, pp. 243–260, 1998.

[17] Y. Ohtake, A. Belyaev, and H.-P. Seidel, "3D scattered data approximation with adaptive compactly supported radial basis functions," in *Proc. of Shape Modeling International*. IEEE Computer Society, 2004, pp. 31–39.

[18] A. Buades, B. Coll, and J. M. Morel, "A non-local algorithm for image denoising," in *Proc. of IEEE Conference on Computer Vision and Pattern Recognition*, 2005, pp. 60–65.

[19] V. Melnik, I. Shmulevich, K. Egiazarian, and J. Astola, "Image denoising using a block-median pyramid," in *Proc. of IEEE International Conference on Image Processing*, vol. 4. IEEE, 1999, pp. 162–166.

[20] J. Mcqueen, "Some methods for classification and analysis of multivariate observations," in *Proc. of the Fifth Berkeley Symposium on Mathematical Statistics and Probability*, 1967, pp. 281–297.

[21] G. Turk, H. Q. Dinh, J. F. O'Brien, and G. Yngve, "Implicit surfaces that interpolate," in *Proc. of International Conference on Shape Modeling & Applications*. IEEE Computer Society, 2001, pp. 62–74.

[22] M. J. L. Orr, "Regularisation in the selection of radial basis function centres," *Neural Computation*, vol. 7, pp. 606–623, 1995.

[23] J. Nakanishi, Y. Kikuchi, S. Inoue, K. Yamaguchi, T. Takarada, and M. Maeda, "Spatiotemporal control of migration of single cells on a photoactivatable cell microarray," *J. Am. Chem. Soc.*, vol. 129, no. 21, pp. 6694–6695, 2007.